UNIVERSITAT POLITÈCNICA DE CATALUNYA BARCELONATECH

UPCommons

Portal del coneixement obert de la UPC

http://upcommons.upc.edu/e-prints

Aquesta és una còpia de la versió *author's final draft* d'un article publicat a la revista *Computational particle mechanics*.

La publicació final està disponible a Springer a través de http://dx.doi.org/10.1007/s40571-018-0204-9

This is a copy of the author 's final draft version of an article published in the journal *Computational particle mechanics*.

The final publication is available at Springer via http://dx.doi.org/10.1007/s40571-018-0204-9

Article publicat / Published article:

Flores, R.M. [et al.] (2018) An implicit unsteady hydraulic solver for suspended cuttings transport in managed pressure wells. *Computational particle mechanics* . Doi:10.1007/s40571-018-0204-9

An Implicit Unsteady Hydraulic Solver for Suspended Cuttings Transport in Managed Pressure Wells

R. Flores[1*], E. Ortega[2], A. Ilin[3], D. Simpkins[4] and E. Oñate[1]

**Corresponding author: rflores@cimne.upc.edu, (+34) 93 401 6038*
[1]International Center for Numerical Methods in Engineering (CIMNE), C/ Gran Capitán s/n, 08034 Barcelona, Spain
[2]Serra Hunter professor at Escola Superior d'Enginyeries Industrial, Aeroespacial y Audiovisual de Terrassa, Universitat Politècnica de Catalunya (ESEIAAT-UPC), C/ Colom 11, 08222 Terrassa, Spain
[3]Weatherford International, 11909 FM 529 Road, Houston, Texas 77041, USA
[4]formerly Weatherford International, Houston, Texas, USA

Abstract. We present a simulation tool for transient events in complex hydraulic networks. The code includes modelling of the transport of suspended cuttings in near-vertical wells. An unstructured finite volume formulation with implicit time integration has been chosen. The unconditional stability of the integrator makes the method suitable for the simulation of transient events over a wide range of characteristic time scales. It handles both very fast transients (e.g. fluid hammer events) as well as the long-term evolution of the well (e.g. hole cleaning operations). The software has been developed to address the need of the oil industry for a robust and efficient predictive tool allowing effective well control in managed pressure drilling operations. The physical modelling follows the standard practices accepted by the industry (e.g. mud rheology computations). The mathematical foundation of the algorithm is described followed by validation cases that illustrate its capabilities and accuracy. Finally, a practical industrial application example is provided to demonstrate the real-world performance of the software.

Keywords*: unsteady, hydraulics, oil well, cuttings transport.*

1 Introduction

The Managed Pressure Drilling (MPD) technique enables precise control of the annular pressure allowing drilling wells that may otherwise not be practical [1,2,3]. Conventional drilling operations, where the mud outlet is at ambient pressure, rely on hydrostatic pressure (regulated by changing the mud density) for well control. In case of narrow margins between pore pressure and formation fracture threshold, conventional drilling can become unfeasible. By maintaining a tighter pressure control (e.g. using choke valves and back-pressure pumps at the surface) MPD can overcome these limitations (see **Fig. 1**).

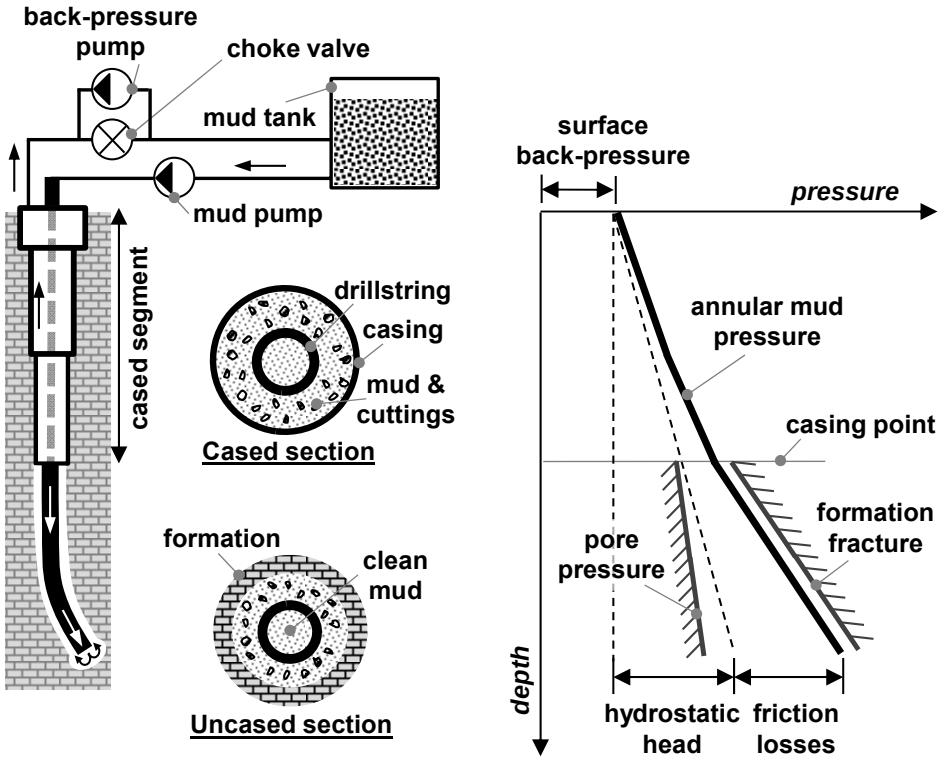

Fig. 1 Simplified schematic of MPD well (left) and Annulus pressure vs. depth diagram (right)

However, to ensure continued safety, an accurate well control strategy with a very short reaction time is needed. This calls for predictive tools capable of computing the response of the well to control inputs (e.g. valve operations or back-pressure pump settings) in near real-time. Moreover, the timescales of the relevant phenomena span many orders of magnitude; from fluid hammer events (10^{-2} s) to hole cleaning activities (hours or days). In all cases the analysis software should be able to provide a solution within the timeframe of a few seconds if safe operation is to be maintained.

Under request from Weatherford International PLC, the International Center for Numerical Methods in Engineering (CIMNE) has developed an unsteady solver for hydraulic networks including modelling of suspended cuttings transport. Weatherford specifically demanded the capability to solve both short and long transients in less than ten seconds using commodity desktop hardware. This would allow future incorporation of the technology in automatic well control systems [4].

A common choice for solving water hammer problems is the method of characteristics [5,6]. However, this explicit technique is best suited for uniformly spaced grids, becomes increasingly complex when the speed of sound in the fluid is not constant and is very inefficient at computing the long-term response of the hydraulic network. On the other hand,

implicit methods, usually based on finite-difference schemes, have been proposed. These allow for larger time steps, thus improving the behaviour when computing slow transients [7,8]. Unfortunately, the computational cost per time step of implicit methods tends to be high, making them inefficient when applied to fluid hammer simulations [9]. Thus, the choice of method (implicit/explicit) usually depends on the time scale of interest (long/short, respectively).

In this paper we present an efficient implicit method suitable for simulation of short and long transients, as well as steady-state simulation. This greatly simplifies the analysis tasks, as a single tool can be applied in all situations. The algorithm is derived from the scheme proposed in [10] for the analysis of fully-incompressible and fully-compressible single-phase flows. The original method has been adapted for slightly compressible fluids (such as drilling muds) and expanded to deal with two-phase flows (mud with suspended cuttings). The details of the numerical scheme are presented, followed by validation cases demonstrating the accuracy and efficiency of the solver. Finally, the most important conclusions are drawn.

2 Governing Equations

Considering Weatherford's operational requirements and the information available from well instrumentation, the following assumptions ware made in the development of mathematical model:

- 1D flow inside a rigid pipe.
- The compressibility of the drilling mud is small.
- The well bore is near-vertical and the velocities in the surface network are high enough for the cuttings to remain suspended.
- The rock cuttings are incompressible and behave as a dispersed phase, where the interactions between the cuttings can be neglected.
- The motion of the suspended cuttings is dominated by viscosity, so the cuttings slip velocity can be computed directly from the local flow conditions. The cuttings velocity is approximately parallel to the pipe axis. Also, the frictional force between cuttings and pipe wall are of minor importance compared with the viscous stresses.

- The temperature field on the well is known at every instant. The effects of temperature on fluid behaviour must be considered, but the temperature itself is part of the input data.
- The well geometry and motion (e.g. drill string displacement) is defined externally and is not affected by the flow field.

The basic equations of 1D fluid flow, see for example [11], have been simplified according to these assumptions. The basic ideas of the scheme [10] have then been applied to the modified equations in order to obtain an efficient numerical model. The changes to the basic equations are summarized next.

2.1 Single-phase conservation statements

The 1D mass balance equation in conservative form for a pipe segment is

$$\frac{\partial \rho}{\partial t} + \frac{\partial (\rho V)}{\partial x} = 0 \ , \tag{1}$$

where ρ denotes the fluid density, V its velocity, x is the streamwise coordinate and t stands for time. The conservative form of the momentum balance is given by:

$$\frac{\partial (\rho V)}{\partial t} + \frac{\partial (\rho V^2)}{\partial x} = -\frac{\partial p}{\partial x} - \frac{f_w}{A} + \rho g_x \ , \tag{2}$$

where p is the fluid pressure, f_w denotes the wall friction force per unit length, A is the pipe cross-section and g_x is the streamwise component of gravity. The left-hand side (LHS) of (2) can be simplified using the continuity equation (1):

$$\frac{\partial (\rho V)}{\partial t} + \frac{\partial (\rho V^2)}{\partial x} = \rho \left(\frac{\partial V}{\partial t} + V \frac{\partial V}{\partial x} \right) + V \left(\frac{\partial \rho}{\partial t} + \frac{\partial}{\partial x} (\rho V) \right) = \rho \left(\frac{\partial V}{\partial t} + V \frac{\partial V}{\partial x} \right) , \tag{3}$$

thus yielding the non-conservative form of the momentum balance

$$\rho \left(\frac{\partial V}{\partial t} + V \frac{\partial V}{\partial x} \right) = -\frac{\partial p}{\partial x} - \frac{f_w}{A} + \rho g_x \ . \tag{4}$$

When the flow velocity is small compared with the speed of sound c, something which is clearly the case in oil wells where V~1 m/s, the continuity equation (1) can be further simplified because the density gradients are negligibly small. We can use the speed of sound to write the density fluctuations in term of pressure gradient, which can in turn be estimated from (4)

$$V\frac{\partial\rho}{\partial x}\approx\frac{V}{c^2}\frac{\partial p}{\partial x}\ ;\ \frac{\partial p}{\partial x}\sim\rho V\frac{\partial V}{\partial x}\rightarrow V\frac{\partial\rho}{\partial x}\sim\frac{V^2}{c^2}\rho\frac{\partial V}{\partial x}=M^2\rho\frac{\partial V}{\partial x}\ , \tag{5}$$

where the Mach number $M=V/c$ has been introduced and $c^2=\left.\frac{\partial p}{\partial\rho}\right|_s$. As the Mach number is very small, the density gradient term in the continuity equation can be safely neglected:

$$V\frac{\partial\rho}{\partial x}<<\rho\frac{\partial V}{\partial x}\ , \tag{6}$$

yielding the acoustic approximation

$$\frac{\partial\rho}{\partial t}+\rho\frac{\partial V}{\partial x}=0\ . \tag{7}$$

In general, whenever the Mach number is small the density gradient terms in the equations can be dropped.

The convective term $\rho V\frac{\partial V}{\partial x}$ on the LHS of (4) is non-linear and complicates the numerical solution of the equations. The key feature of the algorithm developed in [10] is replacing the static pressure *p* with the stagnation pressure p_0

$$p_0=p+q=p+\frac{1}{2}\rho V^2\ , \tag{8}$$

where the dynamic pressure *q* is introduced. Introducing the stagnation pressure in momentum balance equation (4) and recalling that the density gradient can be ignored by virtue of the small Mach number:

$$\rho\frac{\partial V}{\partial t}=-\frac{\partial p_0}{\partial x}-\frac{f_w}{A}+\rho g_x\ . \tag{9}$$

It is a common practice in hydraulic analysis to ignore the convective term in order to simplify the solution scheme. Equation (9) achieves the same effect while remaining exact (within the frame of small compressibility) as the effect of the convective term is contained inside the dynamic part (*q*) of the stagnation pressure.

2.2 Conservation statements for two-phase flow

The method [10] is computationally efficient, but is unfortunately restricted to single-phase flows. Here, the technique is extended to the case of biphasic flow (drilling mud with suspended rock cuttings) simplifying the equations with the model assumptions stated at the beginning of section 2. In the following the subscripts *m*, *s* and *mix* shall refer, respectively, to

the drilling mud, suspended cuttings and the overall mixture. The mass conservation balance for each of the phases is

$$\frac{\partial}{\partial t}\left(\rho_k A_k\right)+\frac{\partial}{\partial x}\left(\rho_k A_k V_k\right)=\phi_k \quad \left(k=m,s\right) \ , \tag{10}$$

where ϕ_k denotes the net mass source (per unit length) of phase k. The subscript k can be either m (mud) or s (suspended cuttings). A_k is the fraction of the cross section occupied by phase k, which can be written in terms of its volume fraction (X_k) as $A_k = AX_k$.

In principle, one momentum balance per phase is required to determine the velocity field. However, in practice, the drag forces experienced by the suspended cuttings cannot be computed accurately. This is due mainly to two issues. First, the cuttings show a wide variation of sizes and shapes, so some representative geometry must be used which gives, at most, a rough approximation of the real drag force. Second, even if all the particles were identical, precise drag correlations are not available for fluids with complex rheology (which is precisely the case of drilling muds). We could further add that for field applications simple models which can be calibrated easily are required, so the particle drag correlations will be approximate at best. With this in mind a simpler and more efficient approach was chosen. As we assumed that the motion of the suspended particles is dominated by viscosity, the particle slip velocity $V_{slip} = V_s - V_m$ can be computed assuming the buoyancy, gravitational and drag forces acting on it are in equilibrium

$$\omega_s\left(\rho_s g_x-\frac{\partial p_0}{\partial x}\right)-D_s=0 \ , \tag{11}$$

where ω_s is the particle volume and D_s is the drag force it experiences (which is a function of its slip velocity). Note that, for convenience, we have assumed $\frac{\partial p_0}{\partial x} \approx \frac{\partial p}{\partial x}$ when computing the buoyancy force. This approximation is valid as long as the variations of cross-section along the duct are smooth. Furthermore, given the approximate nature of the drag estimation, a high level of accuracy is not needed for the pressure gradient. Remark that (11) is an algebraic equation for computing the cuttings slip velocity, which is much easier to solve than the respective momentum balance statement (which is a partial differential equation).

Another equation is needed to complete determine the motion of the system, this could be the momentum balance for the mud, but instead the momentum balance for the overall mixture

has been chosen. The equation is simpler because, when considering the mixture, the forces between the mud and cuttings are internal and do not enter the balance:

$$\rho_{mix}\frac{\partial V_{mix}}{\partial t} = -\frac{\partial p_o}{\partial x} - \frac{f_{mix}}{A} + \rho_{mix} g_x \ , \tag{12}$$

where the average mixture density is $\rho_{mix} = X_m \rho_m + X_s \rho_s$. The equivalent mixture wall force includes the viscous forces and the momentum defect created by the external cuttings sources, if any:

$$f_{mix} = \tau_w l_w + \phi_s \left(V_s - V_{ext} \right) \ . \tag{13}$$

In (13) τ_w is the wall viscous stress, l_w denotes the pipe perimeter and V_{ext} is the velocity of the cuttings when they are introduced in the flow. When the cuttings are fed with low velocity ($V_s > V_{ext}$) they create a drag force on the mixture, because the mixture slows down as it transfer momentum to the external cuttings in order to equalize speeds. For realistic cuttings feed rates this term is small and can be safely ignored. Note that an approximation has been made in (12), because the total pressure p_0 is computed with dynamic pressure of the mud $p_0 = p + \frac{1}{2}\rho_m V_m^2$, while the exact equation would require the dynamic pressure of the mixture. In practice, the error introduced by this approximation is smaller than the uncertainties in the evaluation of the friction forces (given the complex rheology of the mud) so it is not a serious limitation. A further simplification can be made by realizing that if the motion of the particles is dominated by viscous forces, the accelerations of the mud and particles must be similar. This stands to reason because, if the accelerations were significantly different, the particle slip velocities would become large, clogging the well in a very short time. Therefore it is acceptable to assume $\frac{\partial V_{mix}}{\partial t} \approx \frac{\partial V_m}{\partial t}$ and use the equation to compute directly the mud velocity:

$$\frac{\partial V_m}{\partial t} = \frac{1}{\rho_{mix}}\left(\frac{\partial p_o}{\partial x} + \frac{f_w}{A} \right) + g_x \ . \tag{14}$$

2.3 Physical modelling

In order to fully determine the solution $\left(X_m, X_s, V_m, V_s, p_0, \rho_m \right)$ the mass and momentum conservation equations (10) and (14) must be supplemented with additional correlations describing the physical response of the system. These include the mud equation of state, and correlations for the wall friction stresses as well as the cuttings drag force. The models

adopted are explained briefly in the next subsections, check the references provided for a complete description.

2.3.1 Equation of state

Following standard practice in the oil industry, polynomial expressions are used to compute the mud density:

$$\rho_m = a_1 + b_1 p + c_1 p^2 + T\left(a_2 + b_2 p + c_2 p^2\right) , \tag{15}$$

where T denotes temperature and the coefficients a_i, b_i and c_i are material-dependent. The speed of sound can be easily computed from (15)

$$\frac{1}{c^2} = \frac{\partial \rho_m}{\partial p} = b_1 + 2c_1 p + T\left(b_2 + 2c_2 p\right) . \tag{16}$$

Note that, for simplicity, it is possible to use p_0 instead of p when computing the density:

$$\rho_m(p_o,T) \approx \rho_m(p,T) + \frac{\partial \rho_m}{\partial p}\left(p_o - p\right) = \rho_m(p,T)\left(1 + \frac{V^2}{2c^2}\right) = \rho_m(p,T)\left(1 + \frac{M^2}{2}\right) . \tag{17}$$

Given that the Mach number is very small, we conclude from (17) that $\rho_m(p_o,T) \approx \rho_m(p,T)$.

2.3.2 Wall viscous stress

Following the standard practice in the oil industry the friction losses are computed using the procedure outlined in the API RP 13D standard [13] using the Herschel-Bulkley (HB) non-Newtonian fluid model [14]:

$$\tau = \tau_y + k\dot{\gamma}^n , \tag{18}$$

where τ_y is the yield stress, k the consistency factor, n the flow index and $\dot{\gamma}$ denotes the shear rate. The HB model is preferred because it includes, as special cases, Newtonian, Bingham plastic and power-law fluids. To compute the wall friction stress the wall shear rate is first determined with

$$\dot{\gamma}_w = 8\frac{GV}{d_{hyd}} . \tag{19}$$

In the expression above $d_{hyd} = \frac{4A}{l_w}$ is the hydraulic diameter of the duct and the combined geometry shear-rate correction factor G is

$$G \simeq \left(\frac{(3-\alpha)n+1}{(4-\alpha)n} \right) \left(1+\frac{\alpha}{2} \right) , \tag{20}$$

with $\alpha=0$ for the drill pipe and $\alpha=1$ for the annular space. A reference wall shear stress is then given by

$$\tau_w^{ref} = \left(\frac{4-\alpha}{3-\alpha} \right)^n \tau_y + k\dot{\gamma}_w^n , \tag{21}$$

from which the generalized Reynolds number is computed:

$$\mathrm{Re}_G = 8\frac{\rho_m V^2}{\tau_w^{ref}} . \tag{22}$$

The standard [13] gives a semi-empirical correlation for the Fanning friction factor C_f as a function of Re_G. Using the friction coefficient, the wall shear stress can be finally determined:

$$\tau_w = \frac{1}{2}\rho_m V^2 C_f . \tag{23}$$

2.3.3 Cuttings drag force

In order to compute the cuttings slip velocity from relation (11) a correlation for the particle drag force is needed. Following the results of [12] a linear dependency was assumed

$$D_s = D_s\big|_{V_{slip}=0} + \frac{D_s\big|_{V_{term}} - D_s\big|_{V_{slip}=0}}{V_{term}} V_{slip} , \tag{24}$$

where V_{term} is the terminal velocity (in vertical fall) of the particle immersed in the drilling mud. The particle drag at terminal velocity equals the particle weight minus the buoyant force

$$D_s\big|_{V_{term}} = \omega_s \left(\rho_s - \rho_m \right) g . \tag{25}$$

The terminal settling velocity is computed using the Walker and Mayes correlation [15,16]. The method assumes a circular disc of diameter d_s and thickness h_s in flat fall. An empirical correlation for the shear stress at terminal velocity is provided. Following the standard practice in the oil industry, field units are used:

$$\tau_{term} = 7{,}9\sqrt{h_s \left(\rho_s - \rho_m \right)} \quad \left(\frac{\mathrm{lbf}}{100\mathrm{ft}^2} \right) , \tag{26}$$

where the particle size is measured in inches and the densities in lbm/gal. Using the HB fluid model the shear rate at terminal velocity is computed

$$\dot{\gamma}_{term} = \left(\frac{\tau_{term} - \tau_y}{k} \right)^{\frac{1}{n}} \quad \left(\mathrm{s}^{-1} \right) , \tag{27}$$

which in turn yields the apparent viscosity at terminal shear rate:

$$\mu_{term} = 479 \frac{\tau_{term}}{\dot{\gamma}_{term}} \quad (\mathrm{cp}) . \tag{28}$$

Finally, the terminal velocity is

$$V_{term} = 0,0203 \tau_{term} \sqrt{\frac{d_s \dot{\gamma}_{term}}{\sqrt{\rho_m}}} \quad \left(\frac{\mathrm{ft}}{\mathrm{s}} \right) . \tag{29}$$

The particle drag at zero slip velocity is often computed with the expression for the gel strength of a spherical particle

$$D_s \big|_{V_{slip}=0} = \pi d_s^2 \tau_y , \tag{30}$$

however, this expression sometimes yields results incompatible with the Walker and Mayes model (i.e. it predicts $D_s \big|_{V_{term}} < D_s \big|_{V_{slip}=0}$). To address this issue the drag at rest has been computed using:

$$D_s \big|_{V_{slip}=0} = \frac{\tau_y}{\tau_{term}} D_s \big|_{V_{term}} . \tag{31}$$

Using equations (11) and (24) together, the slip velocity of the particles is determined:

$$V_{slip} = \frac{V_{term}}{D_s \big|_{V_{term}} - D_s \big|_{V_{slip}=0}} \left(\omega_s \left(\rho_s g_x - \frac{\partial p_0}{\partial x} \right) - D_s \big|_{V_{slip}=0} \right) . \tag{32}$$

Note that whenever the magnitude of the particle drag is smaller than $D_s \big|_{V_{slip}=0}$ the slip velocity should be set to zero instead of the value predicted by (32).

3 Numerical Model

The algorithm builds on the advantages of Ref. [10], extending the method to include the effect of the suspended cuttings. The solution scheme is staggered, alternating between velocity correction and pressure/concentration correction steps. The spatial discretization is also staggered, using a combination of finite differences for the velocity correction steps and unstructured finite volumes for the computation of pressures and concentrations. The next subsections describe the details of the formulation.

3.1 Problem discretization

3.1.1 Spatial discretization

The spatial discretization scheme is staggered, with the pressures and concentrations evaluated at the nodes of the grid (x_i) and the velocities computed at the midpoints ($x_{i+1/2}$) as shown in **Fig. 2**.

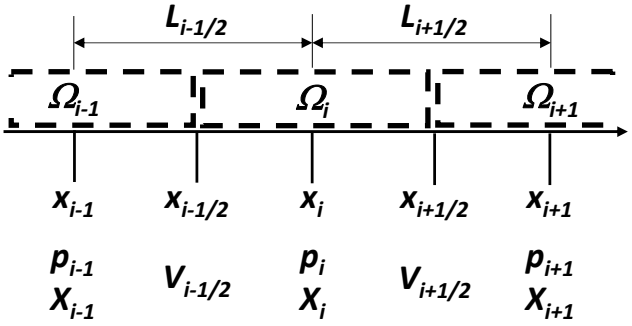

Fig. 2 Staggered spatial discretization

The mud velocity equation (14) is solved using a second-order centered finite difference scheme while the mass conservation equations (10) are solved using a cell-centered finite volume scheme (second-order space accurate too). The cell interfaces are located at the midpoints of neighbouring nodes (where the velocities are computed). The volume of cell *i* is given by:

$$\Omega_i = \frac{L_{i-1/2}A_{i-1/2} + L_{i+1/2}A_{i+1/2}}{2} \ . \tag{33}$$

Note that the pipe cross-sections are defined at the midpoints (i.e. each pipe segment has a constant area, with section changes taking place at the nodes).

3.1.2 Temporal discretization

Due to the complex mud rheology and the nonlinearity of the cuttings slip velocity correlation achieving a converged solution with an implicit integrator can be difficult. To increase the robustness of the solution procedure the backward Euler time integrator is used to advance the equations in time [17]. For the application at hand stability and simplicity were deemed more important than accuracy, so first-order time accuracy was considered an acceptable trade-off. Thus, given a system of ODE's

$$\frac{\mathrm{d}x_j}{\mathrm{d}t} = \phi_j\left(t, x_1, ..., x_n\right) \quad j = 1, ..., n \ ; \tag{34}$$

the unknowns are advanced in time solving the algebraic system

$$\frac{x_j^{t+\Delta t} - x_j^t}{\Delta t} = \phi_j\left(t+\Delta t, x_1^{t+\Delta t}, ..., x_n^{t+\Delta t}\right) \quad j = 1, ..., n \ , \tag{35}$$

where Δt denotes the time step size. To keep the notation as simple as possible, we will assume that all variables are evaluated at the end of the time increment unless explicitly indicated. Values at the start of the time step will be denoted with the superscript ^{0}. Thus, Eq. (35) becomes:

$$\frac{x_j - x_j^0}{\Delta t} = \phi_j\left(t, x_1, ..., x_n\right) \quad j = 1, ..., n \ , \tag{36}$$

3.2 Velocity computation

3.2.1 Mud (mixture) velocity update

The discrete form of the mixture momentum balance equation (12) is

$$\left(L\rho_{mix}\right)_{i+1/2} \frac{\left(V_m - V_m^0\right)_{i+1/2}}{\Delta t} = \left(p_{o\,i} - p_{o\,i+1}\right) - \left(p_{mix}\right)_{i+1/2} + \left(L\rho_{mix} g_x\right)_{i+1/2} \ , \tag{37}$$

where the mixture pressure drop is given by:

$$p_{mix} = \frac{L}{A} f_{mix} = \frac{L}{A}\left[\tau_{mw} l_{mw} + \phi_s \left(V_s - V_{ext}\right)\right] \ . \tag{38}$$

In case localized pressure drops (minor losses) exist, (38) can be augmented with $p_{minor} = K_{loss}\, q$, where K_{loss} is the dimensionless loss factor. This factor can be a function of time (e.g. to simulate valve closures). Equation (37) is nonlinear, as p_{mix} is a function of the velocity, and must be solved iteratively (note that here pressures and concentrations are fixed, they are updated in a later stage of the algorithm). Starting with an approximate value of the mud velocity $\tilde{V}_{m\ i+1/2}^{\ j}$, where j is the iteration counter, we seek an improved solution

$$\tilde{V}_{m\ i+1/2}^{\ j+1} = \tilde{V}_{m\ i+1/2}^{\ j} + \delta^j \tilde{V}_{i+1/2} \ , \tag{39}$$

such that

$$\begin{aligned} &\left(L\tilde{\rho}_{mix}\right)_{i+1/2} \frac{\left(\tilde{V}_{m\ i+1/2}^{\ j} + \delta^j \tilde{V}_{m\ i+1/2} - V_m^0\right)_{i+1/2}}{\Delta t} = \\ &\left(\tilde{p}_{o\,i} - \tilde{p}_{o\,i+1}\right) - \left(\tilde{p}_{mix}^j + \frac{\partial \tilde{p}_{mix}^j}{\partial V_{mix}}\right)_{i+1/2} + \left(L\tilde{\rho}_{mix} g_x\right)_{i+1/2} \end{aligned} \ . \tag{40}$$

The velocity correction for step j is obtained from

$$K^{j}_{i+1/2} \cdot \delta^{j} V_{i+1/2} = b_{i+1/2} - e^{j}_{i+1/2} \ , \tag{41}$$

with

$$\begin{aligned} K^{j}_{i+1/2} &= L_{i+1/2} \frac{L\tilde{\rho}_{mix}}{\Delta t} + \left(\frac{\partial \tilde{p}_{mix}}{\partial V_m} \right)^{j}_{i+1/2} , \\ b_{i+1/2} &= L_{i+1/2} \left(\frac{\tilde{\rho}_{mix} V^{0}_{m}}{\Delta t} + \tilde{\rho}_{mix} g_x \right)_{i+1/2} + \left(\tilde{p}_{0\ i} - \tilde{p}_{0\ i+1} \right) , \\ e^{j}_{i+1/2} &= \left(\frac{L\tilde{\rho}_{mix} \tilde{V}_m}{\Delta t} + \tilde{p}_{mix} \right)^{j}_{i+1/2} . \end{aligned} \tag{42}$$

Using (38) the linearization factor in (42) can be written as:

$$K^{j}_{i+1/2} = L_{i+1/2} \left[\frac{\tilde{\rho}_{mix}}{\Delta t} + \frac{\phi_s}{A} + \frac{l_{mw}}{A} \frac{\partial \tau^{j}_{mw}}{\partial V_m} \right]_{i+1/2} , \tag{43}$$

where it has been assumed that the cuttings slip velocity does not depend on mud velocity. The velocity update step (39) is repeated until convergence is achieved.

3.2.2 Cuttings velocity update

The cuttings slip velocity is obtained solving the algebraic equation (25). If the model for particle drag described in (24)-(32) is used, the equation becomes:

$$\omega_s \left(\rho_s g_x + \frac{\tilde{p}_{0\ i} - \tilde{p}_{0\ i+1}}{L_{i+1/2}} \right) = D_s\big|_{V=0} + \frac{D_s\big|_{V=V_{term}} - D_s\big|_{V=0}}{V_{term}} \left(\tilde{V}_s - \tilde{V}_m \right) . \tag{44}$$

Equation (44) is linear and straightforward to solve once $\tilde{V}$ has been computed.

3.3 Concentration and pressure computation

3.3.1 Mass balance discretization

Using the nomenclature from **Fig. 2**, the rate of change of the mass of a certain species contained inside cell *i* is:

$$\frac{\mathrm{d}}{\mathrm{d}t} \left(\Omega \rho_k X_p \right)_i = \left(F_k \right)_{i-1/2} - \left(F_k \right)_{i+1/2} + \left(L\phi_k \right)_i , \tag{45}$$

where *k* denotes a phase (cuttings or mud) and *F* is the flux at the cell interfaces:

$$F^{i+1/2}_{k} = \left(\rho_k V_k X_k A \right)_{i+1/2} . \tag{46}$$

Applying the backward Euler rule to (45) yields

$$\frac{\Omega_i}{\Delta t}\left(\rho_k X_k - \rho_k^0 X_k^0\right)_i = \left(F_k\right)_{i-1/2} - \left(F_k\right)_{i+1/2} + \left(L\phi_k\right)_i \ . \tag{47}$$

Once again, the equation is nonlinear and must be solved iteratively. To streamline the notation we shall drop the iteration counter and use the tilde to denote only the initial guess. Thus, we will write the improved density and concentration estimates as

$$\rho_k = \tilde{\rho}_k + \delta\rho_k \ ; \ X_k = \tilde{X}_k + \delta X_k \ . \tag{48}$$

Inserting (48) into (47) and discarding high order terms gives

$$\begin{aligned} &\frac{\Omega_i}{\Delta t}\left(\tilde{\rho}_k \delta X_k + \delta\rho_k \tilde{X}_k + \tilde{\rho}_k \tilde{X}_k - \rho_k^0 X_k^0\right)_i = \\ &\left(\delta F_k + \tilde{F}_k\right)_{i-1/2} - \left(\delta F_k + \tilde{F}_k\right)_{i+1/2} + \left(L\phi_k\right)_i \end{aligned} \ , \tag{49}$$

which can be rearranged as:

$$\begin{aligned} &\frac{\Omega_i}{\Delta t}\left(\tilde{\rho}_k \delta X_k + \tilde{X}_k \delta\rho_k\right)_i - \left(\delta F_k\right)_{i-1/2} + \left(\delta F_k\right)_{i+1/2} = \\ &\left(\tilde{F}_k\right)_{i-1/2} - \left(\tilde{F}_k\right)_{i+1/2} + \left(L\phi_k\right)_i - \frac{\Omega_i}{\Delta t}\left(\tilde{\rho}_k \tilde{X}_k - \rho_k^0 X_k^0\right)_i \end{aligned} \ . \tag{50}$$

Note that there are only 2 unknowns per node in (50) because

$$\delta\rho_s = 0 \ ; \ \delta X_m = -\delta X_s \ . \tag{51}$$

The mud density correction can be replaced by the pressure variation through:

$$\delta\rho_m = \frac{\delta p_0}{\tilde{c}_m^2} \ , \tag{52}$$

yielding the update equations for the suspended cuttings fraction and pressure:

$$\begin{aligned} &\frac{\Omega_i}{\Delta t}\left(\rho_s \delta X_s\right)_i - \left(\delta F_s\right)_{i-1/2} + \left(\delta F_s\right)_{i+1/2} = \\ &\left(\tilde{F}_s\right)_{i-1/2} - \left(\tilde{F}_s\right)_{i+1/2} + \left(L\dot{m}_{ext}\right)_i - \frac{\Omega_i}{\Delta t}\rho_s\left(\tilde{X}_s - X_s^0\right)_i \end{aligned} \ , \tag{53}$$

$$\begin{aligned} &\frac{\Omega_i}{\Delta t}\left(\tilde{X}_m \frac{\delta p_0}{\tilde{c}_m^2} - \tilde{\rho}_m \delta X_s\right)_i - \left(\delta F_m\right)_{i-1/2} + \left(\delta F_m\right)_{i+1/2} = \\ &\left(\tilde{F}_m\right)_{i-1/2} - \left(\tilde{F}_m\right)_{i+1/2} - \frac{\Omega_i}{\Delta t}\left(\tilde{\rho}_m \tilde{X}_m - \rho_m^0 X_m^0\right)_i \end{aligned} \ . \tag{54}$$

3.3.2 Flux linearization

In order to compute the updated variables from (53) and (54) the flux increments must be linearized. This will be achieved in two steps, starting with the velocity linearization and following with the complete fluxes.

The change in mud velocity due to pressure and cuttings concentration variations can be estimated from Eq. (37):

$$\left(\frac{L\rho_{mix}}{\Delta t}+\frac{\partial\tilde{p}_{mix}}{\partial V_m}\right)_{i+1/2}\left(\delta V_m\right)_{i+1/2}=\left(\delta p_{o\,i}-\delta p_{o\,i+1}\right)+\left(Lg_x\delta\rho_{mix}\right)_{i+1/2}\ . \tag{55}$$

Experience shows that the last term in the RHS of (55) is extremely important. Neglecting it leads to very poor pressure estimations and lack of convergence. The change in mixture density at the midpoint can be written as:

$$\begin{aligned}&\left(\delta\rho_{mix}\right)_{i+1/2}=\frac{\delta\left(X_m\rho_m+X_s\rho_s\right)_i+\delta\left(X_m\rho_m+X_s\rho_s\right)_{i+1}}{2}=\\&\frac{\left(\delta X_m\rho_m+\delta X_s\rho_s\right)_i+\left(\delta X_m\rho_m+\delta X_s\rho_s\right)_{i+1}}{2}=\\&\left[\delta X_s\frac{\rho_s-\rho_m}{2}\right]_i+\left[\delta X_s\frac{\rho_s-\rho_m}{2}\right]_{i+1}\approx\\&\left(\frac{\rho_s-\rho_m}{2}\right)_{i+1/2}\left[\left(\delta X_s\right)_i+\left(\delta X_s\right)_{i+1}\right]\end{aligned}\ . \tag{56}$$

Note that, due to the low compressibility of the mud, we assume $X_m\delta\rho_m<<\delta X_m\rho_m$. Combining (55) and (56) yields the linearized velocity correction:

$$\begin{aligned}&\left(\frac{L\rho_{mix}}{\Delta t}+\frac{\partial\tilde{p}_{mix}}{\partial V_m}\right)_{i+1/2}\left(\delta V_m\right)_{i+1/2}=\\&\left(\delta p_{o\,i}-\delta p_{o\,i+1}\right)+\left(\frac{Lg_x}{2}\right)_{i+1/2}\left[\left(\rho_s-\rho_m\right)_i\left(\delta X_s\right)_i+\left(\rho_s-\rho_m\right)_{i+1}\left(\delta X_s\right)_{i+1}\right]\end{aligned}\ . \tag{57}$$

The cuttings velocity linearization is obtained adding to (57) the linearized slip velocity computed from (44):

$$\left(\delta V_s\right)_{i+1/2}=\left(\delta V_m\right)_{i+1/2}+\frac{\omega_s}{L_{i+1/2}}\frac{V_{term}}{D_s\big|_{V=V_{term}}-D_s\big|_{V=0}}\left(\delta\tilde{p}_{0\,i}-\delta\tilde{p}_{0\,i+1}\right)\ . \tag{58}$$

The linearized fluxes are obtained from (46), together with the assumption that, due to the low Mach number, density variations are negligible compared with changes in velocity:

$$\delta F_k^{i+1/2} = \left[A\tilde{\rho}_k \left(\tilde{X}_k \delta V_k + \tilde{V}_k \delta X_k \right) \right]_{i+1/2} . \tag{59}$$

In particular, the mud flux variation is

$$\begin{aligned} \delta F_m^{i+1/2} &= \left(\tilde{\rho}_m A\right)_{i+1/2} \left[\left(\tilde{X}_m\right)_{i+1/2} \left(\delta V_m\right)_{i+1/2} + \left(\tilde{V}_m\right)_{i+1/2} \left(\delta X_m\right)_{i+1/2} \right] = \\ &\left(\tilde{\rho}_m A\right)_{i+1/2} \left[\left(\tilde{X}_m\right)_{i+1/2} \left(\delta V_m\right)_{i+1/2} - \left(\frac{\tilde{V}_m}{2}\right)_{i+1/2} \left[\left(\delta X_s\right)_i + \left(\delta X_s\right)_{i+1} \right] \right] ; \end{aligned} \tag{60}$$

and the change is cuttings flux is

$$\begin{aligned} \delta F_s^{i+1/2} &= \rho_s \left(A\right)_{i+1/2} \left[\left(\tilde{X}_s\right)_{i+1/2} \left(\delta V_s\right)_{i+1/2} + \left(\tilde{V}_s\right)_{i+1/2} \left(\delta X_s\right)_{i+1/2} \right] = \\ &\rho_s \left(A\right)_{i+1/2} \left[\left(\tilde{X}_s\right)_{i+1/2} \left(\delta V_s\right)_{i+1/2} + \left(\frac{\tilde{V}_s}{2}\right)_{i+1/2} \left[\left(\delta X_s\right)_i + \left(\delta X_s\right)_{i+1} \right] \right] , \end{aligned} \tag{61}$$

with the variations in mud and cuttings velocities given by (57) and (58).

3.4 Solution procedure

The global solution is obtained following these steps:

1. Initialize all variables with the appropriate initial conditions (or a guess of the solution in the case of time marching to steady-state).
2. Solve for updated velocity with the iterative scheme (41).
3. Update cuttings velocities with (44).
4. Update pressure and cuttings concentration solving the linear system of equations (53) -(54).
5. Go back to step 2 until convergence is achieved.
6. Continue to next time step (update boundary conditions and time increment) and proceed to step 2.

3.5 Convective stabilization

The equations do not contain any diffusion for the transport of cuttings (it is a purely convective phenomenon) so the solution is subject to instabilities (odd-even decoupling). In fact, given that the discretization is second-order space-accurate, Godunov's theorem [18] states that any linear scheme will be subject to spurious oscillations near discontinuities. A simple workaround is to revert to first order space accuracy for the cuttings transport. This

can be easily achieved by altering the interfacial fluxes of cuttings appearing on the RHS of (53). The second-order centered discretization of the flux is:

$$\left(\tilde{F}_s\right)_{i+1/2}^{center} = \rho_s \left(A\tilde{V}_s X_s\right)_{i+1/2} = \frac{\rho_s}{2}\left(A\tilde{V}_s\right)_{i+1/2}\left[\left(X_s\right)_{i+1} + \left(X_s\right)_i\right] . \tag{62}$$

This can be replaced by the first-order upwind approximation to improve stability

$$\left(\tilde{F}_s\right)_{i+1/2}^{upwind} = \rho_s \left(A\tilde{V}_s\right)_{i+1/2}\left(X_s\right)_i , \tag{63}$$

where it has been assumed that the cuttings move from node *i* to node *i+1*. In case of reversed flow the cuttings concentration would be evaluated at node *i+1* (the value at the upstream node must always be chosen). The upwind approximation increases the numerical diffusivity of the cuttings, but this is not considered a limitation. In real cases there is a random distribution of cuttings sizes and shapes, so their slip velocities are not uniform. Therefore, the cuttings transport velocity is variable, causing a streamwise smoothing of the cuttings concentration. The extra diffusion created by the upwind approximation has a qualitatively similar effect, which is not detrimental for the quality of the solution.

3.6 Moving drillstring

For surge/swab simulation (i.e. computing the effect of vertical displacements of the drillstring) the nodes of the grids can be set in motion to reflect the changes in well geometry. The basic equations can be easily modified to account for the drillstring velocity.

3.6.1 Velocity update with moving drillstring

The equations retain the same form as in section 3.2 except that the frictional losses are computed using the equivalent mud velocity given by:

$$V_m^{eq} = \begin{cases} V_m - V_{DP} & \text{for drillpipe} \\ V_m - \dfrac{V_{DP}}{2} & \text{for annulus} \\ V_m & \text{otherwise} \end{cases} , \tag{64}$$

where V_{DP} denotes the drillpipe longitudinal velocity.

3.6.2 Mass balance with moving drillstring

Using an arbitrary Lagrangian-Eulerian (ALE) framework [19], the discrete mass conservation statement (47) becomes

$$\frac{1}{\Delta t}\left(\Omega\rho_p X_p - \Omega^0\rho_p^0 X_p^0\right)_i = \left(F_p^{ALE}\right)_{i-1/2} - \left(F_p^{ALE}\right)_{i+1/2} + \left(L\phi_p\right)_i \ , \tag{65}$$

where the fluxes have been modified to account for the interface velocity:

$$\left(F_p^{ALE}\right)_{i+1/2} = \left[\rho_p\left(V_p - V_g\right)X_p A\right]_{i+1/2} \ . \tag{66}$$

The grid velocity (V_g) at the interface can be interpolated from the nodal velocities:

$$\left(V_g\right)_{i+1/2} = \frac{\left(V_g\right)_i + \left(V_g\right)_{i+1}}{2} \ . \tag{67}$$

4 Application Examples

To illustrate the performance of the method this section presents four benchmark cases for which reference solutions are available, followed by a real-world application example.

4.1 Quasi-steady mud transport test

To validate the mud rheology model the long-term pressure drop along a horizontal pipe segment has been compared with the results from the API RP 13D standard [13]. The relevant problem data are:

- Pipe length: L = 100 m
- Pipe diameter: D = 20 cm
- Mud density: ρ = 1900 kg/m^3
- Speed of sound: c = 1100 m/s
- Fann viscometer readings: θ_3 = 7, θ_6 = 8, θ_{300} = 38, θ_{600} = 63

The characteristic wave propagation time for sound waves along the pipe is $t_c = L/c \sim 0{,}1\,\mathrm{s}$. For time scales long compared to t_c dynamic effects are expected to be negligible and a quasi-steady solution is obtained. The pressure drop across the pipe segment has been ramped linearly from 0 to 5 bar over a period of 1000 s and the results of the numerical model compared with the steady-state predictions from [13]. **Fig. 3** shows the excellent agreement of the numerical model.

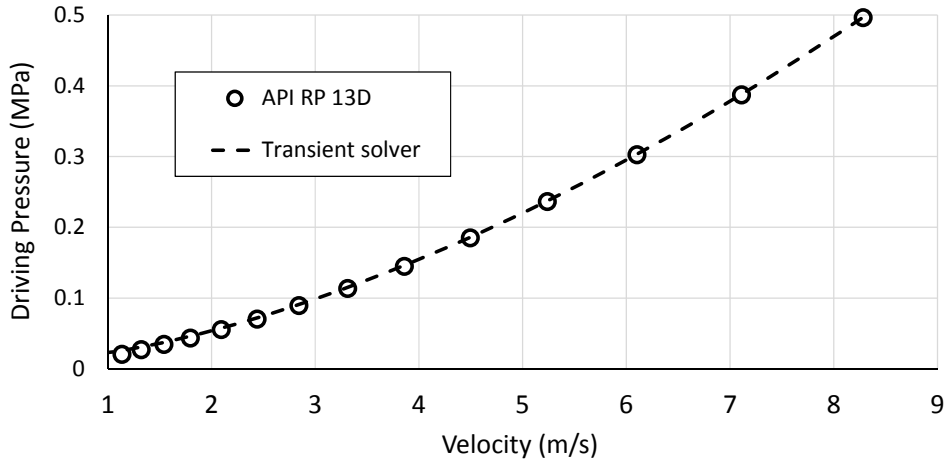

Fig. 3 Quasi-steady pressure drop

4.2 Surge/Swab test

To validate the ALE formulation the case of slow drillstring motion has been analysed. Using an analysis time large compared with the residence time of pressure waves the dynamic effects are negligible and an incompressible steady solution can be used as reference. A 3000 ft (900 m) well with two drillstring sections as depicted in **Fig. 4** is studied.

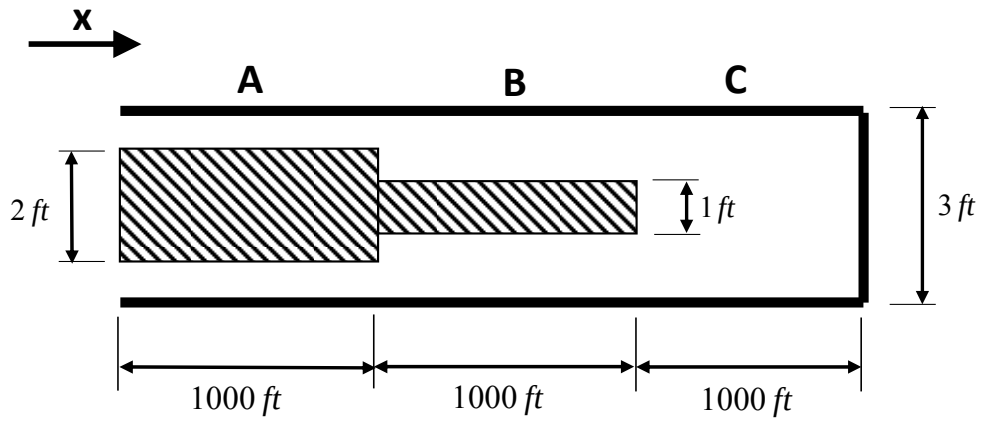

Fig. 4 Moving drillstring test case geometry

The drillpipe is lowered at 1 ft/s (0,3 m/s) during one minute and then raised back to its original position. The hole diameter is 3 ft (90 cm) and the drillpipe diameter varies from 2 ft in section A to 1 ft in section B. The pipe is closed, so mud flows only in the annulus. Assuming full incompressibility the annular flow velocities can be easily estimated:

$$V_A = \frac{2^2}{3^2 - 2^2} V_{DP} = 0,8 \frac{ft}{s} \quad ; \quad V_B = \frac{1^2}{3^2 - 1^2} V_{DP} = 0,125 \frac{ft}{s} \ . \tag{68}$$

The output from the simulation, shown in **Fig. 5** at 10 s steps, matches closely the expected results.

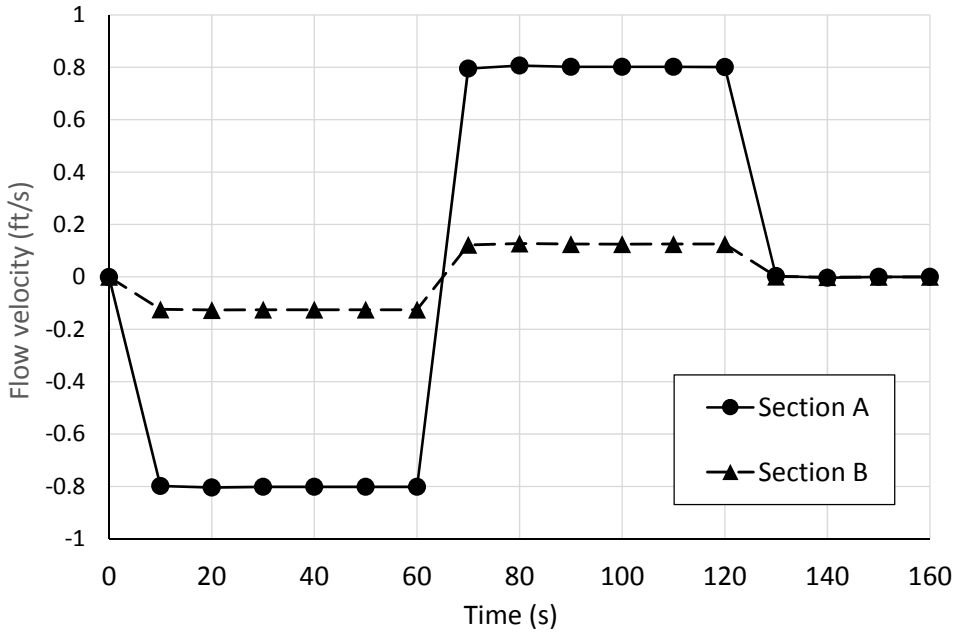

Fig. 5 Outlet flow velocity during surge/swab test case

4.3 Steady-state cuttings transport in vertical annulus test

To validate the solid transport capability, the predictions of the numerical model have been checked against the detailed experimental results from [20]. The transport capabilities of different combinations of drilling muds and cuttings sizes were measured over a range of mud velocities inside a vertical annulus, representative of the conditions found in real wells. The results are expressed in terms of the effective cuttings transport ratio $R = V_s / V_m$; to improve hole cleaning large values of R (i.e. close to 1) are desirable.

The Walker and Mayes method described in section 2.2.3 uses two parameters to describe the cuttings geometry (disk equivalent diameter and thickness). The diameter is taken as the hydraulic diameter of the cuttings, but the equivalent thickness must be calibrated using experimental data, usually by direct measurement of the terminal settling velocity. As this information was not available, the model was calibrated by directly matching the transport ratio from [20] for a single value of the mud velocity. The behaviour of the model was then evaluated varying the mud velocity over a wide range. Interestingly, the disk equivalent thickness was found to depend very weakly on the actual particle size. This is advantageous, as it reduces the need for recalibration of the model when the cuttings characteristics are changed. On the other hand, it was observed that it might be advisable to recalibrate the disk

thickness when muds with vastly different rheological properties are tested under very small anular velocities, i.e. below 30 ft/min (0,15 m/s).

Fig. 6 compares the experimental vs. numerical results for three different cuttings sizes. Please refer to [20] for the complete description of the experimental conditions. The agreement is quite satisfactory over the complete range of velocities (the scatter of the raw experimental measurements is larger than the difference between the two data sets).

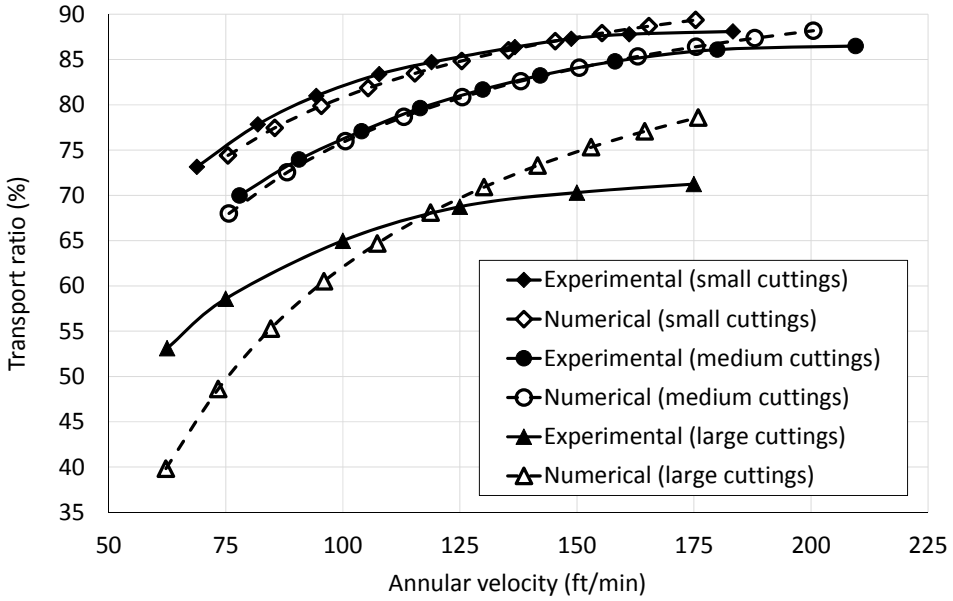

Fig. 6 Effect of cuttings size on transport ratio
(8"x4" annulus, mud#1, 12 ppg mud, 100 rpm drillpipe rotation)

The effects of mud density (**Fig. 7**) and mud rheology (**Fig. 8**) were also studied, yielding satisfactory results (deviations always smaller than the spread of experimental data).

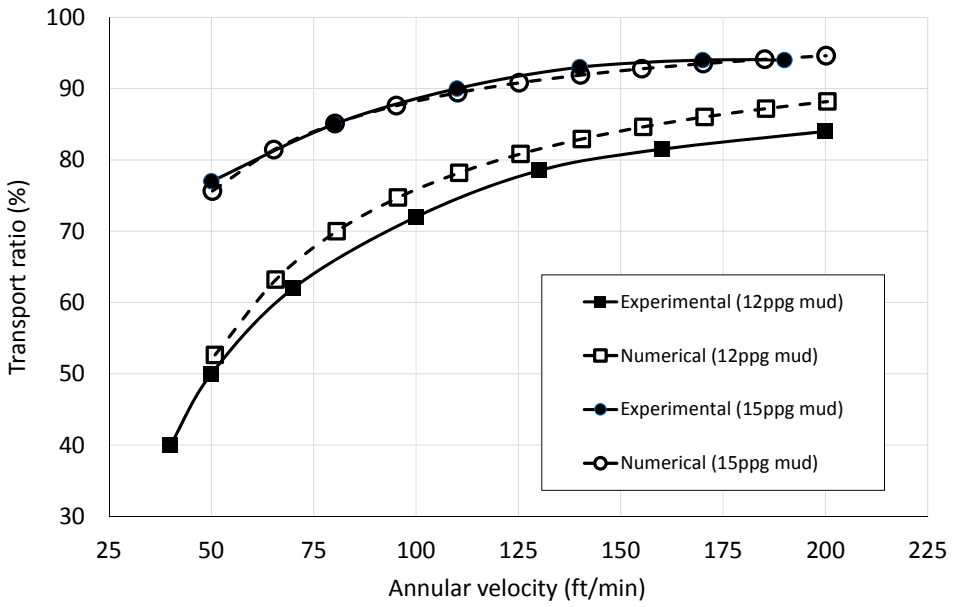

Fig. 7 Effect of mud density on transport ratio
(8"x4" annulus, mud#1, medium cuttings, h=0.45", no drillpipe rotation)

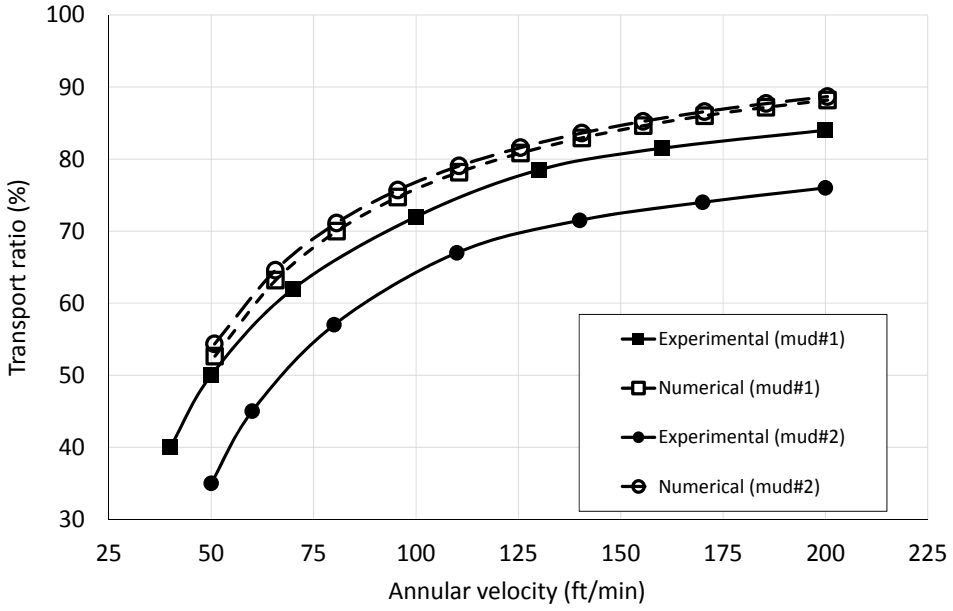

Fig. 8 Effect of mud rheology on transport ratio
(8"x4" annulus, 12 ppg mud, medium cuttings, h=0.45", no drillpipe rotation)

4.4 Fast pressure transient (water hammer) with viscous effects test

The fast-transient (wave tracking) capability has been validated against the experimental study presented in [21]. The setup involves a pipe segment with a constant head water tank on the upstream end and a motorized valve at the outlet (**Fig. 9**). Starting from steady-state

conditions, the valve is closed following a predefined law while the pressure at several points along the duct is monitored.

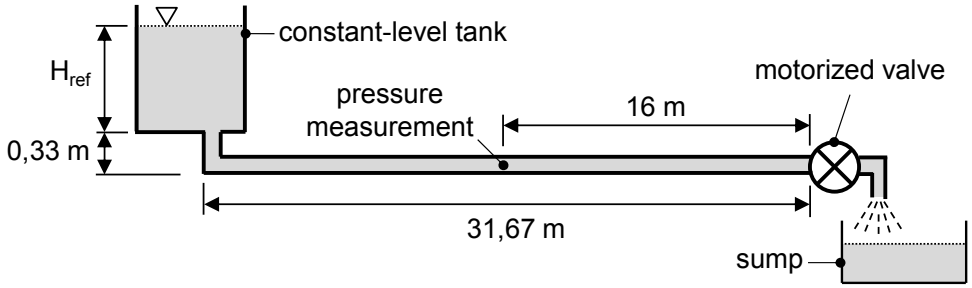

Fig. 9 Experimental setup for water hammer test

Fig. 10 shows a good agreement between the experimental and numerical results for the pressure at the midpoint of the duct. Some small differences must be expected because reference [21] gives the valve closure law in tabulated form. This has been simulated in the code using a minor loss at the pipe outlet. The loss factor is computed at each instant from the valve position table. However, the pressure surge is extremely sensitive to the interpolation algorithm used, causing minor discrepancies.

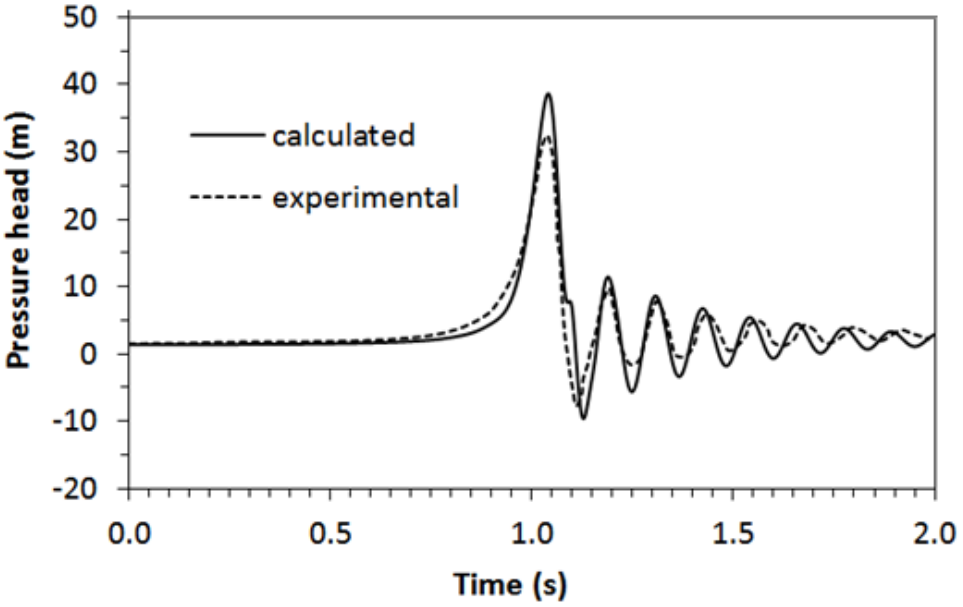

Fig. 10 Pressure evolution at pipe midpoint

4.5 Real-world application example

To illustrate the real-world performance of the algorithm (mostly from the point of view of CPU time, as reliable experimental data from real wells is not freely available) a typical simulation for a 39 400 ft-deep (12 km) pressure managed well is presented. A sudden

actuation of the choke valve while the rig is working in steady conditions is simulated. The computation starts with a time-marching to stationary conditions followed with the fluid hammer event.

The geometry is taken directly from the well logs, and includes a total of 273 cells for the drillpipe, annulus and underbit (the drillstring is partially raised, with the bit positioned at a depth of 6 km). Given that the code has no problem dealing with non-uniform grids (as opposed to programs based on the method of characteristics and explicit finite volume solvers) the cell sizes match exactly the log intervals. Thus, there is no smoothing of the geometry due to transfer of data to a uniform mesh.

The time-marching to steady conditions takes 0,078 seconds in a Core i5-4200U @1.6GHz CPU (note that this is a low-power low-performance processor). The physical time simulated is 13 minutes, thus the computation runs 10 000 times faster than real time. This is possible due to the adaptive time stepping scheme used, which dynamically adjust the time increment to obtain the best compromise between iterative convergence and step size. For our solver it was found that the optimum performance is obtained when approximately 7 global iteration loops are performed for every time step.

Once steady conditions have been reached (that we define as the point where the relative velocity and pressure changes fall below 10^{-6}) a pressure increase of 85 psi (0,59 MPa) lasting 1 s is prescribed at the outlet. The simulation runs 200 additional steps with a time increment of 40 ms to track the wave propagation along the well. This analysis requires 0,14 seconds in the same CPU indicated above.

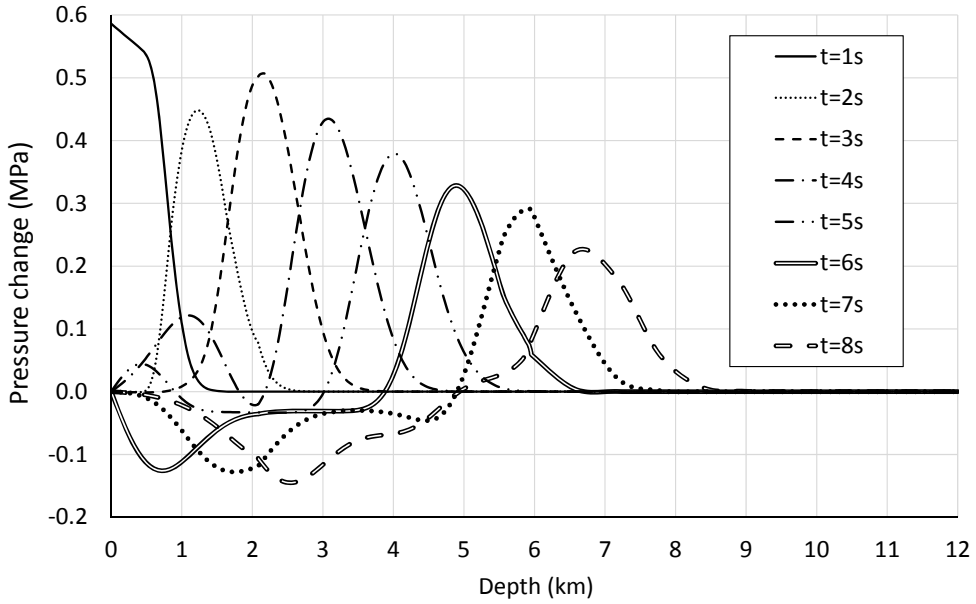

Fig. 11 Pressure surge propagation along annulus and underbit

The evolution of the pressure inside the annulus and underbit at one second intervals is shown in **Fig. 11** (the pressure inside the drillstring was also computed, including jetting losses at the bit, but this data has been removed from the plot for the sake of clarity). Note the anomalous propagation at a depth of 2 km. This is due to the transition from the first to the second casing segment which causes a partial reflection together with an increase in pressure below the area restriction.

5 Conclusions

An unsteady hydraulic network solver for pressure management and cuttings transport in near-vertical oil wells has been presented. Due to an efficient implicit time integrator the code provides a unified framework to simulate long-term evolution of the well (e.g. hole cleaning operations) as well as fast transients (e.g. fluid hammer events during emergency well control). The method accounts for complex drilling mud rheology by means of the industry-standard Herschel-Bulkley model and compressibility effects. By using a formulation based on the stagnation (total) pressure the effect of the convective derivative of the velocity is included implicitly, yielding a simple set of equations that can be solved efficiently. The ability of the method to accurately model several benchmark cases, both steady and transient, has been demonstrated. Finally, a practical application example for a real oil well has been presented, showing the excellent performance of the software. The evolution of the well over

time scales ranging from seconds to hours can be computed in a fraction of a second. This provides a valuable predictive tool to ensure safe drilling operations.

Equivalence between field and SI units

The text includes some field units widely used in the petroleum industry. We list here the equivalence with SI units.

Table 1 Equivalence between petroleum field units and SI.

Magnitude	Symbol	Section	Field unit	SI equivalence
Particle size	d_s, h_s	2.3.3	in	0,0254 m
Density	ρ	2.3.3	lbm/gal (ppg)	119,8264 kg/m^3
Friction stress	τ	2.3.3	lbf/100 ft^2	0,4788026 Pa
Dynamic viscosity	μ	2.3.3	cP	0,001 Pa s
Velocity	V	2.3.3, 4.2	ft/s	0,3048 m/s
Fann viscometer reading	θ	4.1	º (degree)	1º
Length	L, d	4.2, 4.5	ft	0,3048 m
Velocity	V	4.3	ft/min	0,00508 m/s

Acknowledgements

This research was partially funded by Weatherford International.

Conflict of interest statement

On behalf of all authors, the corresponding author states that there is no conflict of interest.

References

[1] Malloy KP et al. (2009) Managed-pressure drilling: what it is and what it is not. IADC/SPE Managed Pressure Drilling and Underbalanced Operations Conference and Exhibition. San Antonio TX, USA

[2] Elliot D et al. (2011) Managed pressure drilling erases the lines. Schlumberger Oilfield Review 23(1): 14-23

[3] van Riet EJ, Reitsma D (2003) Development and testing of a fully automated system to accurately control downhole pressure during drilling operations. SPE/IADC Middle East Drilling Technology Conference & Exhibition. Abu Dhabi, UAE

[4] Guo C et al (2010) Managed pressure drilling micro flux technology allows safer drilling in highly sour reservoirs. International Oil and Gas Conference and Exhibition in China. Beijing, China

[5] Streeter VL, Wylie EB (1998) Fluid mechanics (International 9th revised Ed.). McGraw-Hill Higher Education, New York

[6] Lohrasbi AR, Attarnejad R (2008) Water hammer analysis by characteristic method. American Journal of Engineering and Applied Sciences 1(4): 287-294

[7] Amein M, Chu HL (1975) Implicit numerical modeling of unsteady flows. Journal of the Hydraulics Division - ASCE 101(6): 717-731

[8] Wylie EB, Streeter VL (1970) Network system transient calculations by implicit method. 45th Annual Meeting of the Society of Petroleum Engineers of AIME. Houston TX, USA

[9] Ghidaoui M et al. (2005) A review of water hammer theory and practice. Applied Mechanics Reviews - ASME 58: 49-76

[10] Greyvenstein GP (2002) An implicit method for the analysis of transient flows in pipe networks. International Journal of Numerical Methods in Engineering 53: 1127-1143

[11] Anderson JD (1995) Computational fluid dynamics: the basics with applications. McGraw-Hill, New York

[12] Celigueta MA et al (2016) A FEM-DEM technique for studying the motion of particles in non-Newtonian fluids. Application to the transport of drill cuttings in wellbores. Computational Particle Mechanics 3(2): 263-276

[13] (2010) Rheology and hydraulics of oil-well fluids - API recommended practice 13D (6^{th} Ed.). American Petroleum Institute, Washington-DC

[14] Herschel WH, Bulkley R (1926) Konsistenzmessungen von Gummi-Benzollösungen, Kolloid Zeitschrift 39: 291–300

[15] Walker RE, Mayes TM (1975) Design of muds for carrying capacity. Journal of Petroleum Technology 259: 893-900

[16] Bourgoyne AT, Millheim KK, Chenevert ME, Young FS (1986) Applied Drilling Engineering. SPE Textbook Series, Richardson-TX, pp 173-183

[17] Lomax H, Pulliam TH, Zingg DW (2003) Fundamentals of computational fluid dynamics. Springer, Berlin

[18] Godunov SK (1954) Different methods for shock waves. PhD thesis, Moscow State University.

[19] Stein E, de Borst R, Hughes TJR (Eds.) (2004) Encyclopedia of Computational Mechanics. Wiley, Hoboken-NJ, Vol. 1: Chapter 14

[20] Sifferman TR, Mayers GM, Haden EL, Wahl HA (1974) Drill-cutting transport in full-scale vertical annuli. Journal of petroleum technology, 26(11): 1295-1302

[21] Araya W, Chaudhry M (2001) Unsteady friction in rough pipes. Journal of Hydraulic Engineering 127(7): 607-618